Contents lists available at ScienceDirect

International Journal of Thermofluids

journal homepage: www.sciencedirect.com/journal/international-journal-of-thermofluids

Comparative analysis of heat transfer dynamics in high-intensity focused ultrasound and microwave ablation for cancer treatment

Teerapot Wessapan [a], Pornthip Keangin [b], Phadungsak Rattanadecho [c,*], Nisakorn Somsuk [d]

[a] Department of Mechanical Engineering, Faculty of Engineering, Rajamangala University of Technology Thanyaburi, Pathumthani 12110, Thailand
[b] Department of Mechanical Engineering, Faculty of Engineering, Mahidol University, Nakhon Pathom 73170, Thailand
[c] Center of Excellence in Electromagnetic Energy Utilization in Engineering (CEEE), Department of Mechanical Engineering, Faculty of Engineering, Thammasat University (Rangsit Campus), Pathumthani 12120, Thailand
[d] Department of Industrial Engineering, Faculty of Engineering, Rajamangala University of Technology Thanyaburi, Pathumthani 12110, Thailand

ARTICLE INFO

Keywords:
High-intensity focused ultrasound (HIFU)
Microwave ablation (MWA)
Thermal ablation
Porous biomaterial
Heat transfer

ABSTRACT

This study addresses the crucial need for comparative analyses of High-intensity Focused Ultrasound (HIFU) and Microwave Ablation (MWA) as effective and minimally invasive cancer treatment techniques. Both modalities employ thermal ablation mechanisms but differ fundamentally in their operational physics: HIFU uses focused acoustic waves and MWA uses electromagnetic radiation. Utilizing advanced numerical simulations based on porous media theory, we modeled acoustic and electromagnetic wave propagation and their subsequent interactions with biological tissues. This approach enabled us to accurately depict and analyze the temperature distributions and fluid dynamics during treatment scenarios. Significant results highlighted fundamental differences in the heat transfer mechanisms between the two techniques: for example, under similar power settings, HIFU's focal region reached peak temperatures approximately 2–4 °C higher within the first 10 s, while MWA's thermal footprint extended 20–30 % farther radially. HIFU demonstrated precise, localized heating at the acoustic focus, whereas MWA exhibited broader thermal effects owing to its electromagnetic wave spread. Key findings demonstrate that HIFU provides precision in thermal applications at the risk of requiring exact transducer alignment, whereas MWA's extensive heat spread could treat larger or irregularly shaped tumors but might affect adjacent tissues. Moreover, the flow effects due to the porous nature of tissues significantly influence the heat distribution patterns, with HIFU generating localized and intense heat flux owing to focused acoustic streaming, whereas MWA promotes wider heat spread facilitated by natural convection flows.

1. Introduction

Cancer treatment is a major focus of medical research. Minimally invasive therapies target tumors while reducing radiation and potential damage to healthy tissues. High-intensity Focused Ultrasound (HIFU) and Microwave Ablation (MWA) are minimally invasive techniques that use targeted thermal energy to ablate cancerous tissues and offer alternatives to conventional surgical interventions [1]. These methods have significantly advanced in cancer therapy, offering a non-surgical option for patients who are unsuitable for conventional treatments such as surgery and radiation therapy.

MWA is one of the most commonly used local ablation methods, in which a microwave antenna is used to deliver high-frequency microwaves to tumors [2]. When microwave energy is applied to a tumor, molecules with a dipole moment are forced to continuously realign with the applied frequency, generating kinetic energy and heat within the tumor. HIFU has been quickly accepted in clinical settings as a noninvasive method of tissue ablation. Thermal ablation techniques such as HIFU and MWA utilize heat to induce necrosis in malignant cells without significant harm to the surrounding healthy tissue, making them vital in reducing the recurrence of tumors and extending patient survival. Although other thermal ablation techniques such as Radiofrequency Ablation (RFA), Laser Ablation (LA), and Irreversible Electroporation (IRE) also exist, we focus on HIFU and MWA because they represent distinctly different physical mechanisms (acoustic vs. electromagnetic) and are widely applied in clinical practice. Studying

* Corresponding author.
E-mail addresses: teerapot_w@rmutt.ac.th (T. Wessapan), pornthip.kea@mahidol.ac.th (P. Keangin), ratphadu@engr.tu.ac.th (P. Rattanadecho), nisakorn_so@rmutt.ac.th (N. Somsuk).

https://doi.org/10.1016/j.ijft.2025.101090

Available online 16 January 2025

these two particular modalities under identical conditions offers a clearer understanding of their fundamental heat transfer characteristics, which has not been thoroughly addressed in previous comparative studies.

Despite their growing use, there remains a substantial gap in comparative data, particularly concerning their heat transfer dynamics and resultant biological effects, which are crucial for optimizing their application in clinical settings. This study seeks to address this gap by conducting a comprehensive comparative analysis of heat transfer dynamics in HIFU and MWA. By utilizing advanced numerical simulation techniques grounded in porous media theory [3], this study quantitatively analyzes how each modality influences temperature distributions, specific absorption rates (SAR), and fluid dynamics within treated tissues. These simulations are crucial for understanding the fundamental differences in how HIFU and MWA transfer heat to biological tissues, and their subsequent effects on tumor ablation and surrounding healthy tissues. Comparative analysis focuses on various parameters, such as energy intensity, treatment duration, and tissue properties, to determine the effectiveness and safety of each technique.

Mathematical modeling of thermal phenomena in biological biomaterials, such as tissues, is critical for determining the effectiveness of external heat sources, such as HIFU and MWA, which are essential for predicting treatment outcomes. These models, which are continuously refined over time, are integral to treatment planning because they precisely calculate energy doses and simulate the heat deposition processes necessary for achieving the desired therapeutic effects in targeted tissues. Pennes initially presented a bioheating model of blood-perfused tissue by drawing on the heat transport concept [4]. The influence of fat layer thickness and focal depth on important variables, namely, pressure fields and temperature distributions in tissues during HIFU, has been studied [5]. The temperature distribution was determined by calculating the acoustic pressure field using the nonlinear Westervelt equation and coupling it with Pennes' equation. The experiments were used for comparison with the computational analysis, with a correlation coefficient of 98 %. Advanced equations were employed to develop a creative simulation for investigating the impact of HIFU irradiation patterns on thermal lesions in biological tissues. [6]. The results indicated that the difference in the thermal lesion area between the HIFU irradiation patterns was relatively small, and their lengths and widths were almost the same. Finite element method (FEM) computer simulation was used to assess the effects of MWA treatment on the specific absorption rate (SAR) and necrotic tissue fraction during cancer treatment [7]. According to the numerical data, the input microwave power significantly altered the SAR and temperature distribution. High microwave power increases SAR and boosts temperatures over 50 °C, eliminating cancer cells. Chen et al. [8] conducted a numerical study to investigate the temperature field and damage volume of typical tissues (muscle, fat, and bone) using MWA. The Pennes model and microwave radiation physics were established to predict the possible risks in MWA.

The Pennes model is popular because of its simplicity; however, it has several drawbacks. The main assumption is that the blood perfusion rate is uniform. The countercurrent arrangement between the arteries and veins and the direction of the blood flow were ignored [9]. Several researchers attempted to address these limitations by developing alternative models that deliver accurate results. Mohammadpour and Firoozabad B. [10] developed numerical methods to study the heat transfer and hemodynamics of a porous liver during HIFU ablation. Numerical analysis was used to examine how the hepatic vascular bed affects heat transport in a tumor near the artery. Analysis of the acoustic-thermal-fluid coupled model was conducted to gain insights into the interplay between acoustic pressure, thermal distribution, and fluid flow within the tissue. Researchers have explored heat transport in porous media across local thermal nonequilibrium interfaces. Liver vasculature and porosity were found to significantly affect the cooling effect on the HIFU ablation ability and treatment preparation. HIFU ablation was numerically analyzed to determine the absorption mechanism and nanoparticle-augmented temperature increase [11]. Acoustic streaming affects fluid dynamics and thermal effects in porous tissues during HIFU ablation [12]. This study investigated the impact of tissue permeability, time, and heat transmission models on fluid dynamics and tissue temperature, including an examination of the form and location of the porous tissue heating area. Two heat transmission models were employed: one based on the bioheat equation and the other on a porous medium. These data indicated that tissue flow and temperature were influenced by permeability. Temperature increases in a variety of biological tissues during MWA treatment, for example: Keangin P. and Rattanadecho P. [13] studied the use of the MWA technique for liver cancer treatment through computer simulation using a two-dimensional (2D) axisymmetric model, which included a tumor and normal tissue. The tumor size, porosity, and microwave power were studied. Microwave power input increased the specific absorption rate (SAR) and temperature profiles, whereas tumor porosity and size had little effect. An evaluation of the results of bioheat and porous media approaches in liver cancer during the MWA process based on heat transfer and tissue deformation has been presented [14]. Factors such as tissue properties, temperature-dependent thermal parameters, and local tissue deformation were considered. The results show that the porous media model exhibits significantly different temperature and deformation patterns compared with the bioheat model, suggesting that tissue porosity and permeability play critical roles. Thus, numerical simulation is an invaluable tool for examining the disparities in heat transport properties between HIFU and MWA techniques.

Similar computer methods have predicted heat distributions and optimized treatment options in various biological applications. Hossain et al. [15] used a transient two-phase flow and heat transfer model to study thermal evolutions during multiprobe cryosurgery of hepatic tissues with blood vessels on a thermal study of unstable oscillatory Darcy blood flow in a stenosed artery. Shankar et al. [16] stressed the importance of heat source and thermal radiation effects on biological flows. Rahman et al. [17] also examined drug concentration in ocular tissues using heat transport and metabolic processes in numerical simulations. Additionally, nanoparticles in thermofluids have been studied to improve hyperthermic therapies. Ahmad et al. [18] investigated gold nanoparticles in thermofluids via a porous media for hyperthermic tumor therapy. Advanced mathematical models for complicated biological flow dynamics have been established. Bafe et al. [19] examined the heat and mass transfer of 3D thermo-bioconvective flow of rotating Williamson nanofluid across an exponentially extending surface, including aspects important to biomedicine.

However, the heat transfer dynamics of HIFU and MWA have yet to be explicitly compared under identical conditions, leaving a gap in our understanding of their relative efficiencies and thermal effects in porous tumor tissues. This study examines HIFU and MWA heat transfer dynamics using advanced numerical simulations based on porous media theory. This controlled comparison, using identical tumor models and uniform treatment conditions, shows how each approach affects the tissue microscopically. Different tissue porosities and exposure durations alter tissue temperature distribution and fluid dynamics, according to the study. During ablation, the models calculated the acoustic pressure field, SAR field, and fluid flow, including the temperature distribution. Along with momentum, continuity, and energy equations, acoustic and electromagnetic wave propagation simulations have achieved this. This methodological approach allowed an in-depth comparison of the two techniques under the same operational conditions, providing a unique perspective on their respective advantages and disadvantages in clinical settings. The findings from this comparative study highlight the significant differences in heat transfer characteristics between HIFU and MWA, offering valuable insights into their respective benefits and drawbacks as cancer treatment options.

2. Problem formulation

The problem addressed in this study arises from the growing interest and need within the medical community to optimize local tumor ablation techniques, such as HIFU and MWA, which represent innovative and feasible cancer therapy options. Although HIFU and MWA have potential benefits, they are also associated with significant risks. These techniques may displace the ablative site, leading to coagulative necrosis that assumes atypical shapes, thereby increasing the risk of damage to the adjacent healthy tissues. Furthermore, the lack of direct comparative studies assessing and contrasting the therapeutic effects and specific heat transfer characteristics of HIFU and MWA has left a gap in our understanding of whether there are significant differences between these methods in terms of treatment efficacy and safety. This study aims to fill this knowledge gap by comprehensively comparing the heat transfer dynamics and therapeutic outcomes of HIFU and MWA, thereby elucidating any substantial disparities in their physical treatment profiles and effects on targeted tissues. Fig. 1 illustrates the physical domain of the problem. Fig. 1(a) shows a schematic diagram and model details of the HIFU treatment, and Fig. 1(b) shows a schematic diagram and model details of the MWA treatment. This study comprehensively compared the heat transfer characteristics of two treatment methods: HIFU and MWA.

3. Methods and model

In this section, the methods and models used are focused on comparing the effects of HIFU and MWA treatments on energy absorption, flow dynamics, and heat transfer in porous tissues through local ablation. Initially, the research involved calculating the induced acoustic pressure for HIFU and electromagnetic wave propagation for MWA in the targeted tissues. Subsequent analyses assessed how this absorbed energy influenced the temperature increase and associated transport processes. Utilizing a consistent tumor model under identical conditions allowed a preliminary evaluation of the effectiveness of each technology. The parameters for the study were chosen based on prior research on thermal ablation, with the aim of establishing guidelines for assessing potential thermal injury thresholds associated with these ablation techniques.

3.1. Mathematical model

The physical model utilized in this study was a fluid-saturated structure represented as a porous medium. The porous tissue model comprises two parts: the fluid-phase vascular region and the solid-phase extravascular region [20]. A porous tissue model with a tumor was used to study the heat transfer characteristics of HIFU and MWA during cancer treatment. The tissue was isotropic with unchanging characteristics. Blood saturates the pore space of porous tissue, which has no main

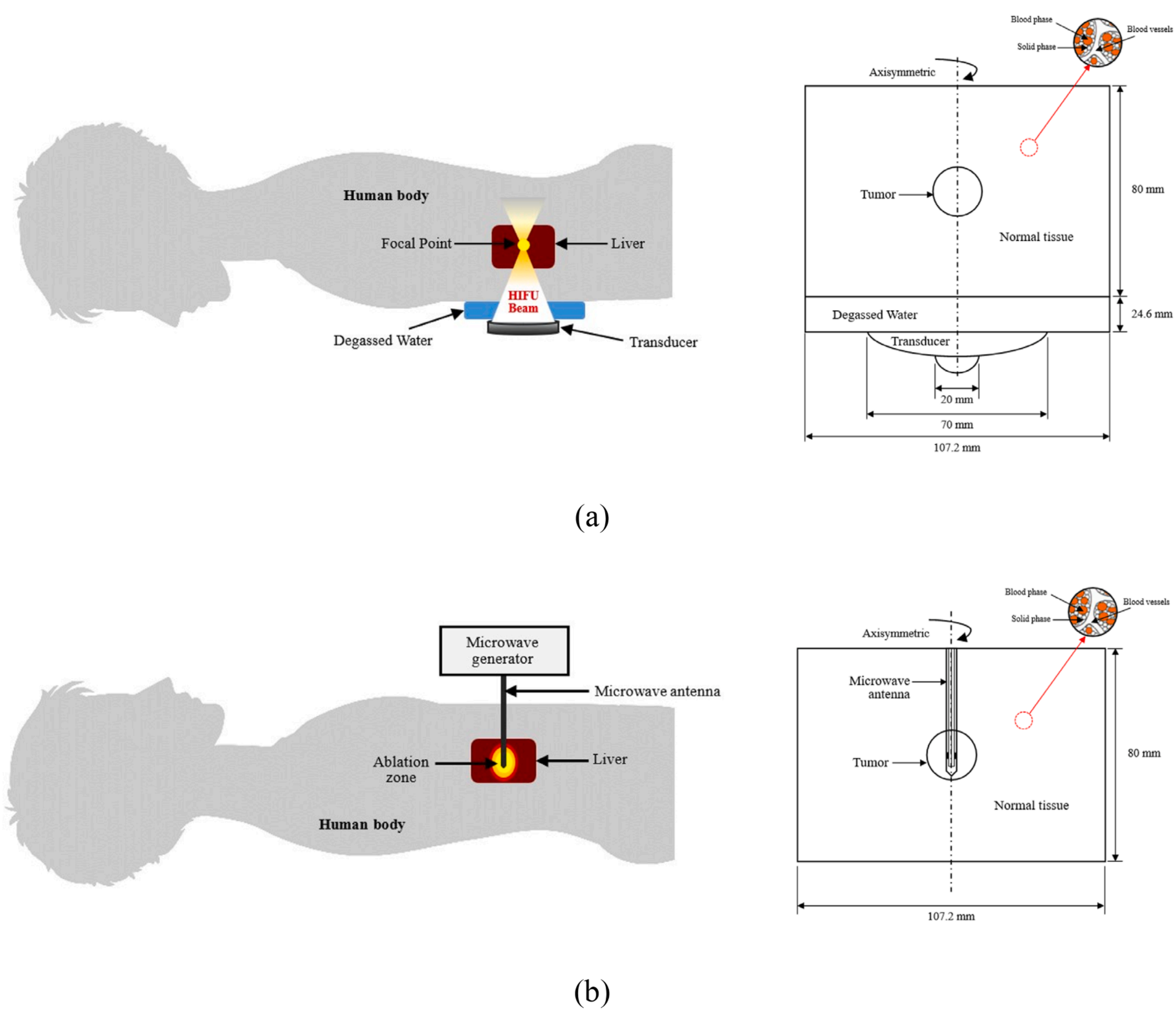

Fig. 1. The physical domain of the problem: (a) Schematic diagram and model details of HIFU treatment and (b) Schematic diagram and model details of MWA treatment.

vessels. No chemical reactions or phase changes were observed in the tissues. This study optimized the processing time and resolution by representing the vertical cross-section of a 3D model with a 2D axisymmetric model. Table 1 lists the dielectric and thermal properties of tissues [13,21]. Fig. 1(a) shows the schematic diagram and model details of the HIFU treatment. The ultrasonic source employed was a spherically focused, single-element piezoelectric transducer featuring a 70-mm aperture and 20-mm central hole. The focal length was 62.64 mm, and the operating frequency was 1.0 MHz. The cylindrical tissue model had a diameter of 107.2 mm and a length of 80 mm. Degassed water was positioned 24.6 mm from the point of contact. Additionally, Fig. 1(b) illustrates a schematic diagram and model details of the MWA treatment utilized in this study. In this study, a single-slot microwave antenna was inserted into a tissue model to transmit microwave power directly to tumor-associated cells, leading to its destruction. A microwave antenna with a diameter of 1.79 mm was chosen for interstitial MWA therapy because of its narrow profile, which minimizes its impact on the surrounding healthy tissues. Three main components were constructed: inner conductor, dielectric, and outer conductor. The antenna included a ring-shaped slot that was 1 mm wide. This slot is cut from the outer conductor, extending 5.5 mm from the short-circuit tip to allow efficient treatment of deep-seated tumors. The antenna operated at 2450 MHz, which is the standard frequency for the MWA process. Based on a preliminary study, the dimensions and dielectric properties of the single-slot microwave antenna are listed in Table 2 [13].

3.2. Equation for acoustic wave propagation analysis for HIFU treatment

The mathematical model calculates the acoustic pressure using the acoustic wave equation. Similar to the work of Bhowmik et al. [22], the analysis used a 2D axisymmetric model to simplify the acoustic wave propagation simulation. The model also assumes that the tissue acoustics are constant. The axisymmetric Helmholtz equation in cylindrical coordinates describes the acoustic wave propagation. This equation describes acoustic wave transmission in the model and simplifies the wave equation governing the acoustic pressure field [22]:

$$\frac{\partial}{\partial r}\left[-\frac{r}{\rho}\left(\frac{\partial p_s}{\partial r}\right)\right]+r\frac{\partial}{\partial z}\left[-\frac{1}{\rho}\left(\frac{\partial p_s}{\partial z}\right)\right]-\left[\left(\frac{\varpi}{c_0}\right)^2\right]\frac{rp_s}{\rho}=0 \tag{1}$$

where p_s is the acoustic pressure (Pa), ϖ is the angular frequency (rad/s), ρ is the density (kg/m^3), c_0 is the speed of sound (m/s), and r and z are the radial and axial coordinates, respectively.

3.2.1. Boundary conditions for acoustic wave propagation analysis

An axial symmetry boundary condition was imposed on the axisymmetric model along the symmetry axis at $r = 0$:

$$\frac{\partial p_{s,r}}{\partial r}=0 \tag{2}$$

The inward normal acceleration (a_n) (m/s^2) was applied to the surface of the acoustic transducer as the external source term.

$$-n\cdot\left[-\frac{1}{\rho_c}(\nabla p_s-q)\right]=a_n \tag{3}$$

Because the tissue model was located in the tissue container, the tissue walls were considered rigid, and the outer edges of the domain were treated as sound-hard boundary conditions:

$$-n\cdot\left[-\frac{1}{\rho_c}(\nabla p_s-q)\right]=0 \tag{4}$$

where q denotes the dipole source (N/m^3), and n denotes the normal vector.

To simplify the problem, the dipole source term was assumed to be zero.

Table 1
The dielectric and thermal properties of the tissue [13,21].

Properties	Normal tissue	Tumor	Blood
Relative permittivity, ε_r (-)	43	58.3	48.16
Electric conductivity, σ (S/m)	1.69	2.54	2.096
Density,ρ(kg/m^3)	1030	1058	1040
Specific heat capacity, c_p (J/kg·K)	3600	3960	3960
Thermal conductivity,k (W/m·K)	0.497	0.45	0.57

3.3. Equations for electromagnetic wave propagation analysis for MWA treatment

The propagation of electromagnetic waves is represented by 2D axially symmetric cylindrical coordinates (r–z). A transverse electromagnetic (TEM) field characterizes an electromagnetic wave propagating along a single-slot microwave antenna. A transverse magnetic (TM) field was utilized to represent an electromagnetic wave within the tissue in a manner analogous to previous studies [13]. The wall of the single-slot microwave antenna was modeled as a perfect electric conductor. The scattering boundary condition shortened the outer surface of the porous tissue. The electromagnetic fields propagating over the single-slot microwave antenna associated with the time-varying TEM wave were evaluated in 2D axially symmetric cylindrical coordinates, as follows:

Electric field:

$$\overrightarrow{E}=e_r\frac{C}{r}e^{j(\varpi t-kz)} \tag{5}$$

Magnetic field:

$$\overrightarrow{H}=e_\phi\frac{C}{rZ}e^{j(\varpi t-kz)}, \tag{6}$$

where

$$C=\sqrt{\frac{ZP}{\pi\cdot\ln(r_{outer}/r_{inner})}} \tag{7}$$

In these equations, Z represents the wave impedance (Ω), P denotes the input microwave power (W), r_{inner} and r_{outer} refer to the dielectric's inner and outer radius (m), respectively. Additionally, f denotes the frequency (Hz), $k=2\pi/\lambda$ represents the propagation constant (m^{-1}), and λ denotes the wavelength (m).

A transverse magnetic (TM) field was used to describe the characteristics of the electromagnetic waves within the porous tissue domain, as follows:

$$\nabla\times\left(\left(\varepsilon_r-\frac{j\sigma}{\varpi\varepsilon_0}\right)^{-1}\nabla\times\vec{H}_\phi\right)-\mu_r\gamma_0^2\vec{H}_\phi=0, \tag{8}$$

where ε_0 represents the permittivity of free space with a value of 8.8542×10^{-12} F/m, ε_r denotes the relative permittivity (-), σ denotes the electrical conductivity (S/m), μ_r represents the relative permeability (-), and γ_0 represents the free-space wave number (m^{-1}).

3.3.1. Boundary condition for acoustic wave propagation analysis

TM-wave propagation with various input microwave powers was assigned to the inlet of the single-slot microwave antenna. An axis symmetry boundary condition was used at $r = 0$:

3.4. Equations for heat transfer and flow analysis

Absorption of acoustic and electromagnetic waves by biological tissues converts these waves into heat. To fully examine the transport processes outlined in this section, we evaluated coupled models of wave propagation, heat transfer, and fluid (blood) flow in a porous tissue. The assumptions helped to analyze heat transmission and blood flow. This

Table 2
Dimensions of a microwave antenna [13].

Materials	Dimensions (mm)	Dielectric properties		
		Relative permittivity, ε_r (-)	Electric conductivity, σ (S/m)	Relative permeability, μ_r (-)
Inner conductor	0.135 (radial)	–	–	–
Dielectric	0.335 (radial)	2.03	0	1
Outer conductor	0.460 (radial)	–	–	–
Catheter	0.895 (radial)	2.1	0	1
Slot	1.000 (wide)	1	0	1

process does not modify the tissue phase. No chemical reactions were observed in these tissues. The tissue is a thermally isotropic, homogeneous, fluid-saturated porous medium. The following equation describes the transient tissue heat transport:

The following equation describes the transient tissue heat transport:

3.4.1. Energy equation (Porous media model)

$$(\rho c)_{eff}\frac{\partial T}{\partial t} - \nabla\cdot\left(k_{eff}\nabla T\right) = -(\rho c)_b u\cdot\nabla T + Q_{met} + Q_{ext}, \tag{9}$$

where

$$(\rho c)_{eff} = \left(1-\varepsilon_p\right)(\rho c)_s + \varepsilon_p(\rho c)_b \tag{10}$$

represents the overall heat capacity per unit volume of the tissue, and

$$k_{eff} = \left(1-\varepsilon_p\right)k_s + \varepsilon_p k_b \tag{11}$$

denotes the overall thermal conductivity [3,21].

Referring to the equation above, ρ represents the density of tissue (kg/m^3), T denotes the tissue temperature (°C), k denotes the thermal conductivity of tissue (W/m. K), c represents the tissue heat capacity (J/kg K), t represents the time (s), u denotes the flow velocity (m/s), ε_p represents the tissue porosity (-), Q_{met} refers to the metabolic heat production (W/m^3), and Q_{ext} refers to the external heat source (W/m^3). The effective value, solid tissue phase, and blood phase are replaced by the subscripts *eff, s,* and *b*, respectively.

3.4.2. Bioheat equation

The energy equation based on the bioheat model is as follows:

$$\rho c_s\frac{\partial T}{\partial t} - \nabla\cdot(k_s\nabla T_s) = \rho c_b\omega_b(T_b - T_s) + Q_{met} + Q_{ext}, \tag{12}$$

where ω denotes the blood perfusion rate (1/s). Because it requires fewer assumptions than the traditional bioheat model, the porous-media approach appears to be the most feasible way to model the transport phenomena in any biological material [3,4,12].

3.4.3. Fluid flow in porous tissue

Fluid movement within the porous tissue was described using the Brinkman-extended Darcy model [23]. The equations describing the fluid flow in a porous tissue are as follows:

Continuity equation:

$$\nabla\cdot u = 0 \tag{13}$$

Momentum equation:

$$\left(\frac{\rho}{\varepsilon_p}\right)\frac{\partial u}{\partial t} + \left(\frac{\mu}{\kappa}\right)u = -\nabla p + \nabla\cdot\left[\left(\frac{1}{\varepsilon_p}\right)\left(\mu\left(\nabla u + (\nabla u)^T\right)\right)\right] + \rho\beta\left(T - T_{ref}\right)g + F \tag{14}$$

where p represents the pressure (Pa), μ denotes the dynamic viscosity (N. s/m^2), g represents the gravitational acceleration (m/s^2), β refers to the volume expansion coefficient (1/K), T is the local temperature (°C), T_{ref} is a reference temperature (°C), and g is the gravitational acceleration (m/s^2), and F represents the body force induced by acoustic streaming (N/m^3), calculated as follows:

$$F = \frac{2\alpha}{c_0}I \tag{15}$$

The buoyancy effects resulting from temperature differences were modeled using the Boussinesq approximation, which assumes that the fluid density varies slightly with temperature but remains constant with respect to pressure.

Nondimensionalization is a process where governing equations are transformed into dimensionless forms by scaling variables such as pressure, length, and time using characteristic values. This approach eliminates units, reduces the complexity of the equations, and enhances numerical stability during simulations. This transformation facilitates the comparison of results across different systems and ensures consistency in computational analyses. These nondimensional parameters help compare different configurations and enhance computational efficiency, and have been commonly adopted in prior studies (e.g., [16, 20]).

3.4.4. Boundary conditions for heat transfer and flow analysis

The external surfaces of the tissue model were considered to be constant at 37 °C. An open boundary condition, permitting the fluid to enter and exit the computational domain, was applied to the external boundaries of the porous tissue domain for flow analysis.

$$n\cdot\left[-p2i + \left(\frac{1}{\varepsilon_p}\right)\mu\left(\nabla\cdot u + (\nabla\cdot u)^T\right)\right] = -f_0\cdot n, \tag{16}$$

where n is the normal vector of the boundary, f_0 is the normal stress (N/m^2), and i is the identity matrix.

The initial temperature was considered to be constant throughout the model.

$$T(t_0) = 37^{\circ}C \tag{17}$$

3.5. Calculation procedure

The calculation procedure for this study was organized systematically using the finite element method (FEM), a numerical technique used to address complex governing equations, as well as the defined initial and boundary conditions. A 2D axisymmetric geometry was discretized using a triangular mesh, with finer elements concentrated around the focal region of the HIFU transducer and the vicinity of the MWA antenna tip to capture steep gradients in temperature and flow variables. Utilizing the adaptive mesh refinement approach, this method allowed for enhanced precision and efficiency in numerical simulations by dynamically adjusting the mesh density in response to spatial and temporal variations in the solution. Numerical convergence was ensured by conducting a mesh independence study, where solutions were compared for different mesh densities to verify that the results remained consistent. To implement and execute these calculations, COMSOL™ Multiphysics software was employed to provide a robust platform for simulating intricate phenomena occurring within the tissue model during exposure to both HIFU and MWA techniques.

4. Results and discussion

A comprehensive comparison between the HIFU and MWA techniques was conducted using computational models to analyze their respective heat transfer dynamics, fluid flow, and energy field distributions within the tumor and surrounding tissue. The tissue properties presented in Table 1 were obtained directly from prior studies, ensuring that the simulations accurately reflected the behavior of biological tissues during thermal ablation treatments. The results provide valuable insights into the potential advantages and limitations of each technique, especially when considering key parameters such as tumor porosity and treatment duration.

4.1. Model verification

The accuracy of the current numerical model was verified by comparing the numerical and experimental results of prior research, with particular emphasis on the work of Huang et al. [24] for HIFU treatment and Yang et al. [25] for MWA treatment. Both validation cases were aimed at simulating temperature increases within tissues under similar exposure conditions. In the case of HIFU, the numerical model used a bioheat approach to simulate the temperature increase in the tissue, and the results from the present study were compared with those of a previous study (Fig. 2(a)). The frequency of the HIFU transducer was set to 1.1 MHz, and the properties of the liver tissue were consistent with those reported in previous studies. The maximum temperature increase reached approximately 1 °C at 1 s of exposure, showing good agreement with the results of previous work, thus confirming the accuracy of the HIFU simulation. For MWA, the validation was conducted by simulating the temperature rise in the liver tissue at distances of 4.5 mm and 9.5 mm from the microwave antenna (Fig. 2(b)). A comparison with the experimental data of Yang et al. demonstrated that the results of the present study closely matched the temperature profiles obtained from the experimental measurements. The maximum temperature increase is consistent with the values observed by Yang et al., particularly for the first 40 s of the ablation process. This agreement between the numerical results and experimental data validates the present numerical model, ensuring its reliability in simulating both HIFU and MWA treatments in biological tissues.

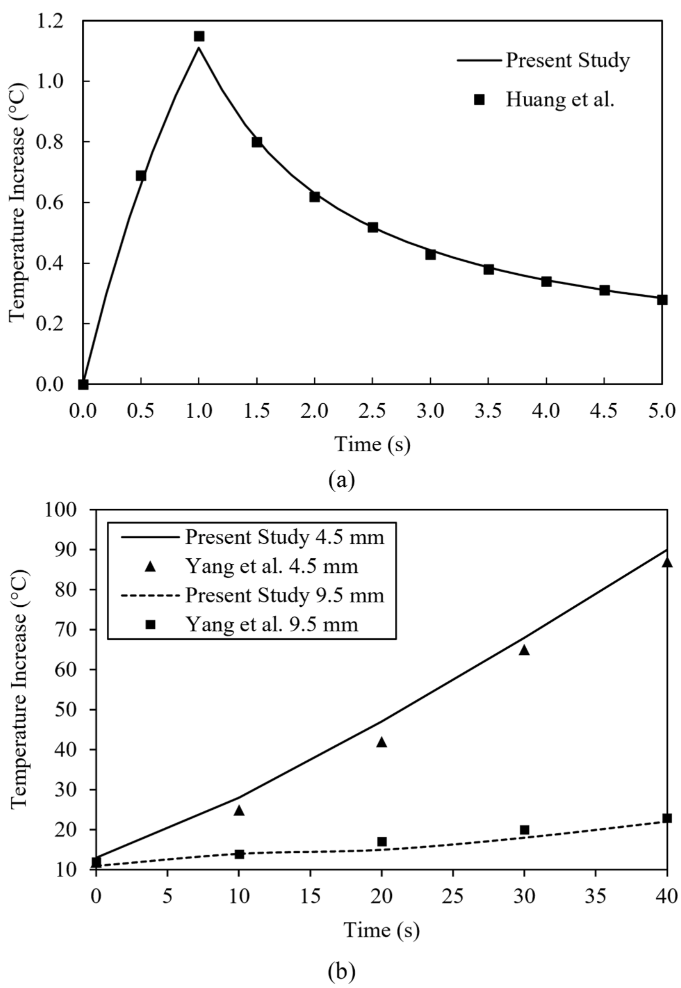

Fig. 2. Validation of the numerical models by comparing the temperature increase and various exposure times: (a) Comparison between temperature increase-time distributions obtained from the present numerical study and obtained by Huang et al. [24] of HIFU treatment and (b) Comparison between temperature increase-time distributions obtained from the present numerical study using bioheat model and experimental data by Yang et al. [25] of MWA treatment.

4.2. Spatial distribution of energy fields

The spatial distribution of the energy fields for both HIFU and MWA was analyzed to understand the impact of external energy sources on the tumor and the tissue immediately surrounding the tumor. The contour plots in Fig. 3 illustrate the energy distributions for both the acoustic pressure field (HIFU) and electric field (MWA), where the central circle represents the tumor.

In Fig. 3(a), the acoustic pressure field in the HIFU shows a focused energy field, with the highest pressure concentrated at the focal point of the tumor ($r = 0$). The pressure reaches values close to 1.8×10^6 Pa near the center, gradually decreasing as it moves outward from the focal region. This concentration indicates that HIFU generates localized energy deposition, effectively targeting the tumor and reducing damage to the adjacent healthy tissue. The focused nature of the HIFU energy field results in precise thermal ablation, which is ideal for small, well-defined tumor regions.

In Fig. 3(b), the electric field generated by the MWA exhibits a more spread-out distribution, covering a broader area around the tumor. The electric field reaches a maximum of approximately 1.07×10^5 V/m near the antenna, gradually decreasing as it spreads through the surrounding tissue. Unlike the tightly focused energy in HIFU, MWA's electric field of MWA extends further into the surrounding tissue, suggesting a larger area of influence. This broader coverage makes MWA suitable for treating larger or irregularly shaped tumors. However, it may also affect adjacent healthy tissues owing to its wider heat distribution.

A comparison of the energy fields for both techniques demonstrates their complementary capabilities. HIFU offers precise, localized treatment for small tumors, whereas MWA provides a broader energy distribution for ablating larger regions. These characteristics indicate that the selection between HIFU and MWA may be contingent on tumor size and shape, along with the requirement for precision and broad tissue coverage.

4.3. Heat transfer dynamics using different models

The heat transfer dynamics in tumors subjected to HIFU and MWA were analyzed using both the bioheat and porous media models under the same power of 5 W and tissue porosity of 0.3. Fig. 4 illustrates that the temperature rise in HIFU is initially greater according to the Bioheat Model. However, the Porous Media Model yields a marginally lower temperature owing to the pronounced forced convection from acoustic streaming, which redistributes the heat across a broader volume, consequently reducing the temperature at the focal point. By contrast, for the MWA, the temperature predicted by the porous-media model was higher than that predicted by the Bioheat Model, as illustrated in Fig. 4. This difference arises because the much lower flow velocity in the MWA (Fig. 5) reduces convective heat transfer, allowing more heat to

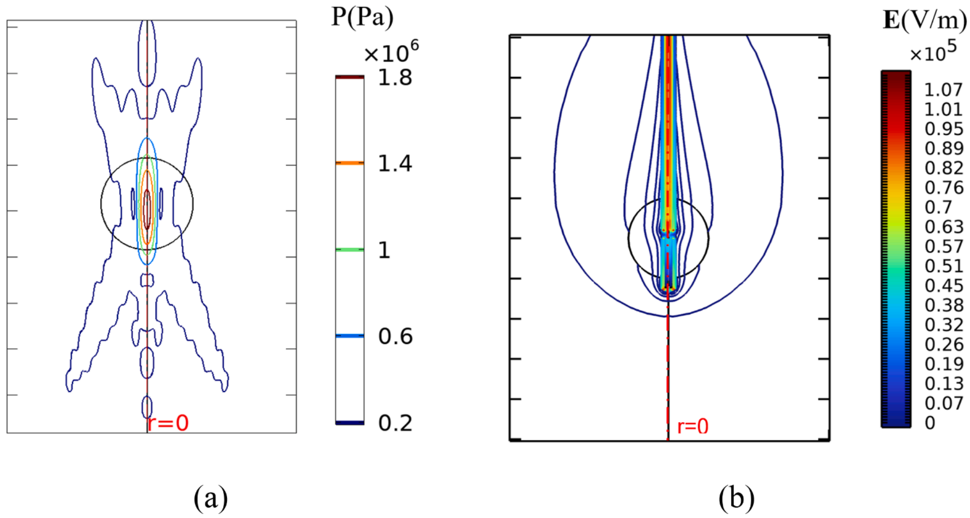

Fig. 3. Contour showing the distribution of 5 W external energy sources of HIFU and MWA: (a) Acoustic pressure field (Pa) of HIFU and (b) Electric field (V/m) of MWA (porosity tissue and tumor of 0.3).

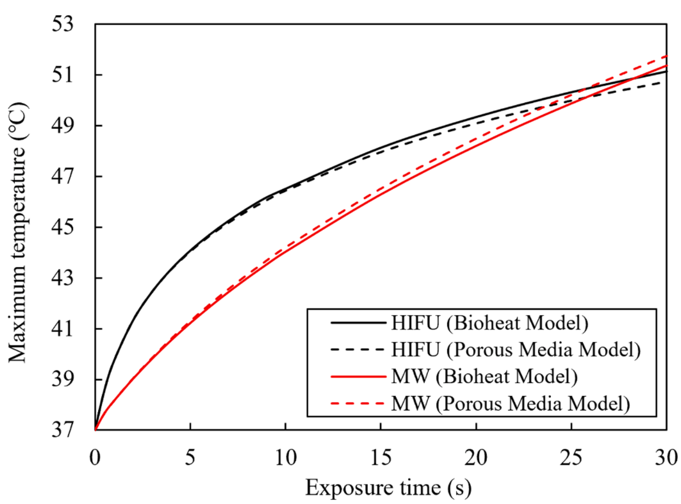

Fig. 4. Maximum temperature vs. exposure times in the tumors treated with HIFU and MWA using the bioheat model and the porous media model (at the same power of 5 W, porosity tissue and tumor of 0.3).

accumulate around the microwave antenna, leading to higher temperatures. The heat is primarily transferred through conduction because the natural convection in the MWA is relatively weak compared with the forced convection in the HIFU.

The spatial distribution of temperature in Fig. 5 further highlights the differences between the two techniques. For HIFU (Fig. 5(a)), the heating is localized around the focal point, reaching a maximum temperature of 50.74 °C with the Porous Media Model, while the Bioheat Model predicts a slightly higher temperature. The flow induced by acoustic streaming within the porous media model resulted in a slight upward peak temperature shift along the flow direction. In MWA (Fig. 5 (b)), the thermal distribution encompasses a wider area, reaching a maximum temperature of 51.75 °C. The extensive heat distribution in MWA renders it appropriate for the treatment of larger tumors; however, it may pose a danger to adjacent healthy tissues. The Porous Media Model provides a more precise depiction of heat transfer by integrating the effects of tissue porosity and convective flow. This is particularly relevant for HIFU, where convective heat transfer plays a significant role in reducing the temperature at the focal point and shifting the peak temperature slightly upward, as shown in Fig. 5(a). The shape of the temperature distribution also changed compared to that of the heat model, indicating that acoustic streaming caused heat to disperse over a region. Conversely, the lower convective effects in the MWA result in heat accumulation near the antenna because the temperature rise is mostly dictated by conductive heat transfer.

4.4. Impact of tumor porosity on treatment efficacy

Fig. 6 shows a comparison of the velocity profiles between HIFU and MWA at an exposure time of 10 s. In Fig. 6, the streamline patterns reveal distinct differences between HIFU and MWA, owing to the underlying physics of each technique. In HIFU (Fig. 6(a)), circular streamlines were observed around the tumor driven by acoustic streaming, which is a secondary flow generated by the nonlinear interaction of ultrasound waves with fluid particles. At $\varepsilon_{\text{tumor}} = 0.2$, the flow is relatively symmetrical with distinct circular patterns forming around the tumor. As porosity rises to $\varepsilon_{\text{tumor}} = 0.3$, the vortices become more pronounced and the flow strength escalates, signifying improved convective heat transmission. At $\varepsilon_{\text{tumor}} = 0.4$, the flow patterns become more diffuse, exhibiting intensified flow around the tumor, signifying an increased fluid velocity. Fig6b shows the streamline patterns of the MWA technique for varying porosities, demonstrating the distinct characteristics of fluid flow around the tumor. At $\varepsilon_{\text{tumor}} = 0.2$, the flow is relatively weak with minimal circular motion around the tumor, signifying that the heat transfer is primarily governed by conduction. As porosity increases to $\varepsilon_{\text{tumor}} = 0.3$, the streamline shows slightly more developed vortices, with flow moving more dynamically around the tumor, enhancing convective heat transfer. At $\varepsilon_{\text{tumor}} = 0.4$, the flow intensifies with more pronounced vortices forming around the tumor, leading to a higher fluid velocity and stronger convective effects. This progression suggests that increased porosity amplifies fluid motion and contributes to more efficient heat distribution in the MWA treatment, although the flow remains weaker than that of HIFU because of the absence of acoustic streaming.

Tumor porosity plays a critical role in determining the efficacy of thermal treatments such as HIFU and MWA. Fig. 6 illustrates that the fluid velocity profiles for both HIFU and MWA exhibited considerable variance in relation to tumor porosity (ε). For HIFU (Fig. 6(a)), increasing tumor porosity from 0.2 to 0.4 results in a noticeable rise in maximum fluid velocity (u_{max}), from 2.23×10^{-4} m/s to 2.16×10^{-3} m/s, due to reduced fluid resistance within the tumor tissue. This increase in velocity leads to more effective convective heat transfer, which can enhance the localized heat distribution. Conversely, for MWA (Fig. 6

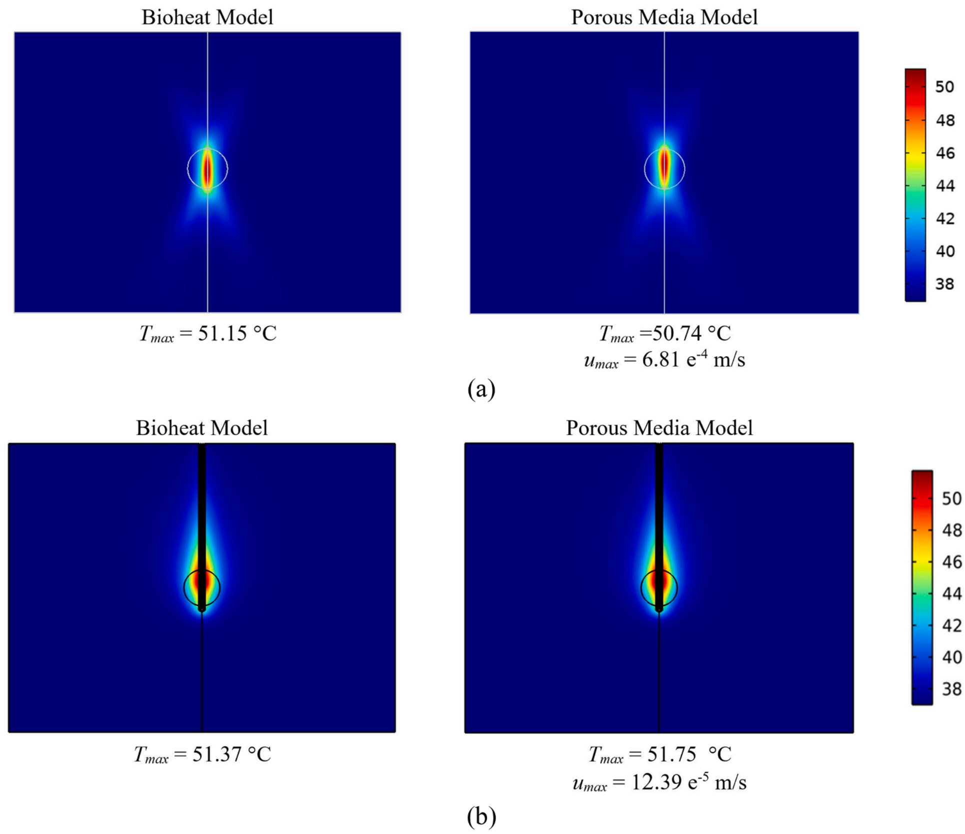

Fig. 5. Temperature distributions generated by Bioheat model and porous media model at exposure time of 30 s: (a) HIFU and (b) MWA.

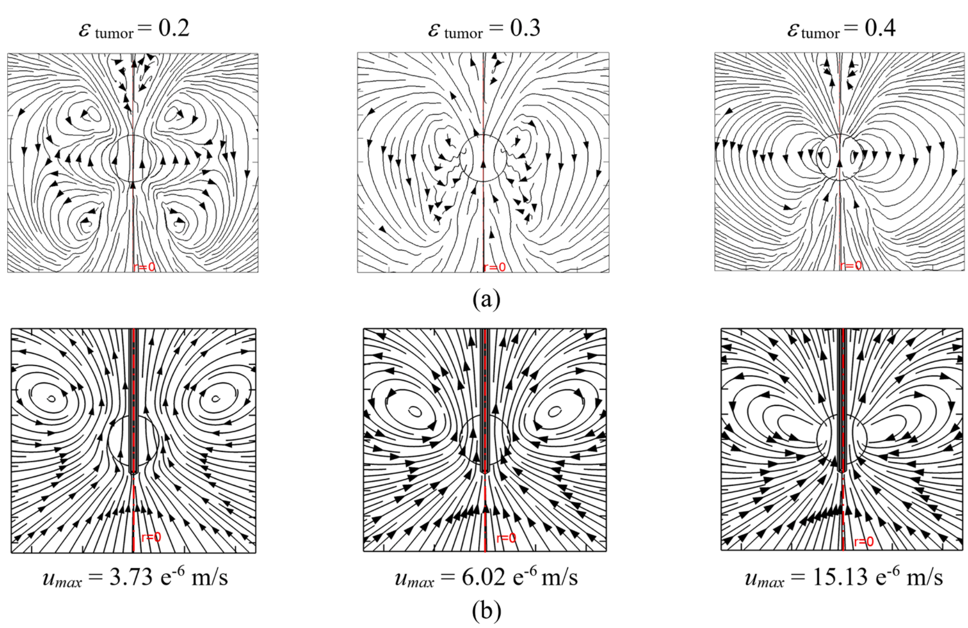

Fig. 6. Comparison of velocity profile between HIFU and MWA at an exposure time of 10 s: (a) HIFU and (b) MWA.

(b)), the fluid velocity also increased with increasing porosity; however, the values were much lower, indicating a more subdued effect of convection compared with HIFU. The velocity for MWA at a pore size of 0.4 reaches only 15.13 × 10^{-6} m/s, signifying that conduction remains the primary heat transfer mode.

Fig. 7 presents a comparison of the peak tumor temperatures between the HIFU and MWA treatments across varying tumor porosity levels with an initial exposure duration of 10 s. This figure illustrates the varying heat sensitivities of the two depigmentation techniques with increasing tumor porosity. The MWA treatment shows a relatively stable peak temperature of around 44.5 °C, regardless of the tumor's porosity, indicating that its heating mechanism remains consistent during the early phase of treatment. In contrast, HIFU's maximum temperature decreases as porosity increases, dropping from approximately 46.5 °C at a porosity of 0.2 to about 43.5 °C at a porosity of 0.4. This difference in behavior underscores the distinct effects of porosity on the thermal

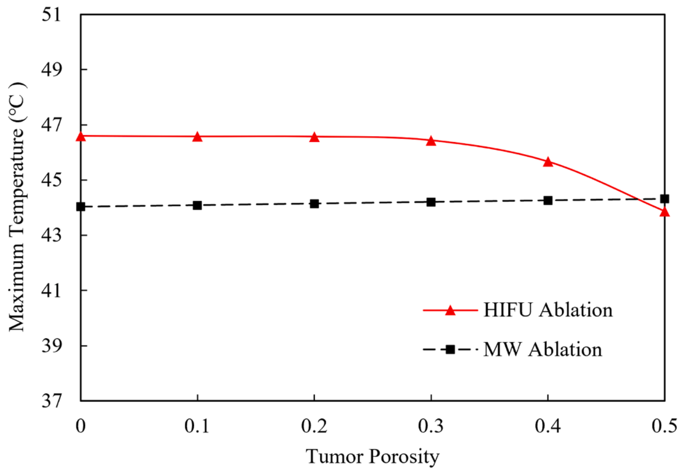

Fig. 7. Comparison of maximum tumor temperature at various tumor porosities between HIFU and MWA at an exposure time of 10 s.

efficacies of HIFU and MWA.

The stability of the MWA temperature response is attributed to its primary heating mechanism, which relies on the absorption of electromagnetic energy. This mechanism remains largely unaffected by changes in tumor porosity because the dielectric heating process is uniform and unaffected by the initial convective heat transfer at early exposure times. In contrast, HIFU's temperature decrease in HIFU with higher porosity is driven by the enhanced convective heat transfer caused by acoustic streaming, which is a forced convection effect unique to HIFU. This phenomenon allows fluid movement within the porous tissue to dissipate heat more effectively, thereby reducing the temperature at the focal point. Fig. 8 corroborates this conclusion, demonstrating that the HIFU flow velocity significantly increases with the porosity (Fig. 8(a)), enhancing the convective heat transfer, whereas the MWA flow velocity remains substantially lower (Fig. 8(b)), leading to a stable temperature profile. Consequently, in the first exposure phase, HIFU exhibited greater sensitivity to variations in tissue porosity than MWA, which remained stable owing to the delayed onset of spontaneous convection.

Continuing from the analysis of Fig. 7, which highlights the impact of tumor porosity on the maximum temperature achieved during ablation treatments, Fig. 8 provides a deeper insight by comparing the maximum flow velocities within the tumor tissue subjected to HIFU and MWA across various porosity levels and exposure times. This figure is crucial for comprehending how fluid dynamics in porous tissues affect heat transmission mechanisms, and consequently, the thermal efficacy of the two tissue ablation techniques.

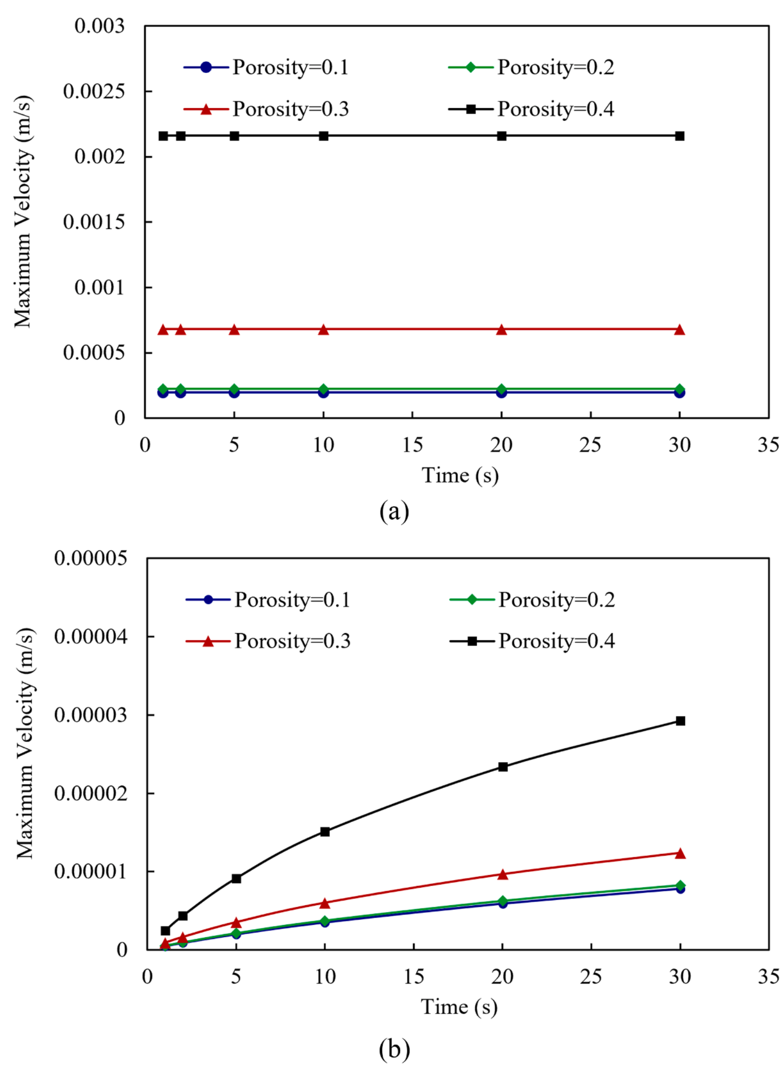

Fig. 8. Comparison of maximum flow velocity at various tumor porosities at various time:
(a) HIFU and (b) MWA.

Fig. 8(a) shows the peak flow velocities associated with HIFU treatment. As the tumor porosity rises from 0.2 to 0.4, the peak flow velocity increased significantly. At higher porosity levels, the linked pore gaps inside the tissue became more pronounced, facilitating enhanced fluid movement driven by acoustic streaming. The flow velocities for HIFU were substantially greater than those for MWA, reaching magnitudes on the order of 10^{-4} m/s. This elevated flow velocity indicates a robust forced convection effect that promotes convective heat dissipation away from the focal zone. Consequently, this enhanced convective heat transfer in HIFU at higher porosity levels leads to a reduction in the maximum tumor temperature, as shown in Fig. 7.

Fig. 8(b) shows the peak flow velocities for the MWA treatment. The flow velocity in MWA is markedly lower, on the order of 10^{-6} m/s, and progressively rise with time and with enhanced porosity. The marginal increase in flow velocity signifies that spontaneous convectioninduced by temperature gradientsis the primary mechanism facilitating fluid movement in the MWA. However, at an early exposure time of 10 s, natural convection did not develop sufficiently to significantly affect heat transfer. Consequently, the convective effects in the MWA were minimal during the initial stages, leading to stable maximum temperature profiles across different porosities, as shown in Fig 7.

These flow velocity profiles elucidate the contribution of convective heat transfer mechanisms to the thermal behavior observed in both ablation techniques. In HIFU, the immediate onset of acoustic streaming produces significant convective cooling, particularly in tissues with higher porosity, leading to a decrease in the maximum temperatures. In MWA, the delayed development of natural convection limits its influence on the temperature, leading to a stable thermal profile despite variations in tissue porosity. Understanding these dynamics is crucial for enhancing treatment protocols and achieving more effective tumor ablation.

4.5. Temporal evolution of temperature distribution

Fig. 9 presents the temperature distributions within the tumor tissue during exposure durations of 10 s, 20 s, and 30 s for both modalities, with a tumor porosity (ε_{tumor}) of 0.3. This figure shows the temporal heat distribution throughout the tissue, and facilitates a comparative evaluation of the thermal impact of each technique.

Fig. 9(a) shows the temperature distribution for HIFU treatment. At 10 s, the maximum temperature (T_{max}) reaches 46.44 °C, concentrated in the focal point of the ultrasound beam. Over time, the temperature rises to 49.09 °C at 20 s and 50.74 °C at 30 s, with the heat zone extending along the flow direction due to acoustic streaming. The shape of the heat zone evolved over time and elongated in response to the convective flow generated by acoustic streaming, as shown in Fig. 8. This elongated pattern highlights the role of high flow velocities ($u_{max} = 6.81 \times 10^{-4}$ m/s) in redistributing heat along the axis of the focused ultrasound, which was previously demonstrated in Fig. 6.

Fig. 9(b) shows the temperature distribution for the MWA treatment. At 10 s, the T_{max} is 44.20 °C, located in the antenna's center. As exposure time increases, the temperature rises to 48.49 °C at 20 s and 51.75 °C at 30 s. However, unlike HIFU, the configuration of the heating zone in MWA stays predominantly consistent, expanding uniformly outward rather than elongating. This radial expansion is consistent with the conduction-dominated heat transfer, where the impact of the fluid flow is insignificant. The flow velocity for MWA, as shown in Fig 8(b), is significantly lower ($u_{max} = 6.02 \times 10^{-6}$ m/s at 10 s), reflecting the limited role of convection in heat transfer for this modality. As a result, the heating zone of the MWA expanded symmetrically, maintaining a consistent shape while increasing in size over time.

In summary, computational analysis compared HIFU and MWA in terms of heat transfer dynamics, fluid flow, and thermal phenomena in the tissue domains of embedded tumors. The models were experimentally validated to confirm their reliability. HIFU produces localized heat by concentrated energy deposition, which is ideal for precise targeting, whereas MWA produces a broader energy distribution suited for larger tumors but with greater risk to nearby tissues. The porous media model proved to be more accurate by including the influences of tissue porosity and convective flow, which significantly impacted HIFU's efficacy of HIFU, resulting in a reduction in the peak temperature with increased porosity. In contrast, the MWA temperature remained stable across the porosity levels, driven mainly by conduction. These results emphasize the importance of considering tissue properties and fluid dynamics when optimizing thermal ablation techniques.

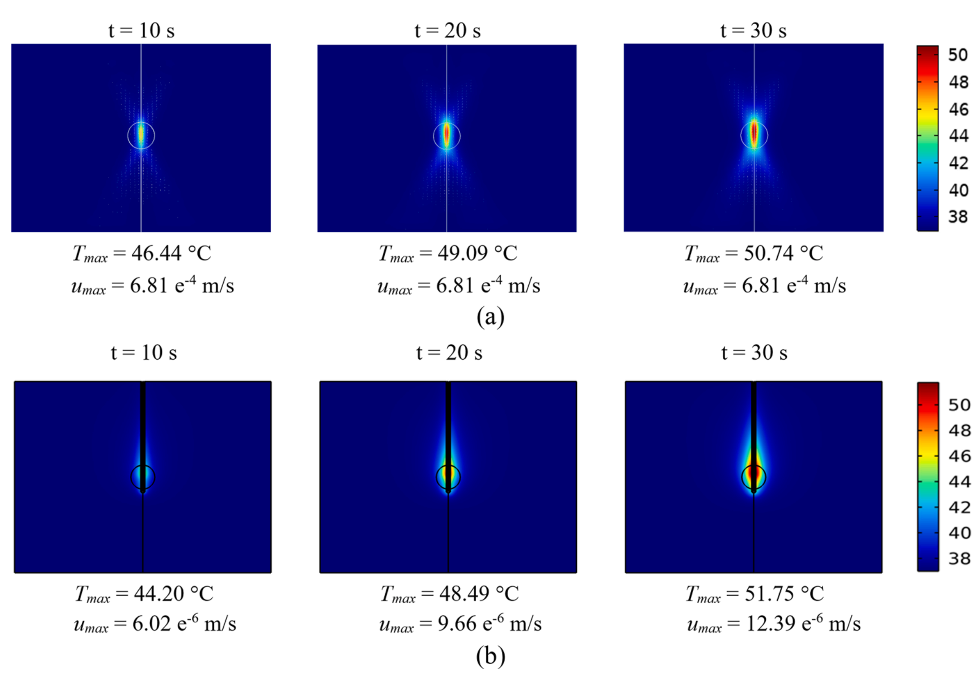

Fig. 9. Temperature distribution in the tissue ($\varepsilon_{tumor} = 0.3$, $\varepsilon_{tissue} = 0.3$) at various exposure time using: (a) HIFU and (b) MWA.

5. Conclusions

This study provided a thorough comparative analysis of HIFU and MWA treatments, focusing on the heat transfer dynamics within porous tumor tissues. Through advanced numerical simulations based on the porous media theory, the research revealed significant differences in energy distribution, fluid flow, and thermal behavior between the two ablation techniques. It was shown that HIFU may produce localized heating due to concentrated acoustic waves, with a pronounced convective impact from acoustic streaming, resulting in improved heat distribution in the more porous tissue and lower peak temperatures as the porosity increased. In contrast, MWA produced a broader and more uniform thermal profile, mostly influenced by conductive heat transfer, showing relative insensitivity to tumor porosity during the initial treatment stages.

This study highlighted the importance of considering tissue characteristics, particularly porosity and fluid dynamics, when selecting and optimizing thermal ablation techniques for cancer therapy. Based on the findings, HIFU is recommended for small, well-defined tumors that require precise and localized heating, especially where adjacent tissue sparing is critical. Conversely, MWA is better suited for larger or irregularly shaped tumors due to its broader heating zone and higher tolerance to tumor geometry variations. A deeper understanding of heat transfer mechanisms and tissue properties will guide treatment planning and enhance therapeutic outcomes, thereby advancing the development of minimally invasive cancer treatments.

Nomenclatures

a	acceleration (m/s^2)
c	specific heat capacity (J/(kg K))
c_0	speed of sound (m/s)
E	electric field intensity (V/m)
F	body force (N/m^3)
f_0	normal stress (N/m^2)
g	gravitational acceleration (m/s^2)
H	magnetic field (V/m)
I	acoustic intensity (W/m^2)
i	identity matrix
k	thermal conductivity (W/(m K))
n	normal vector
P	input microwave power (W)
p	pressure (N/m^2)
Q	heat source (W/m^3)
T	temperature (K)
u	velocity (m/s)
t	time (s)
Z	wave impedance (Ω)
Greek letters	
α	acoustic absorption coefficient (m^{-1})
β	volume expansion coefficient (1/K)
ε_0	permittivity of free space (F/m)
ε_p	porosity
ε_r	relative permittivity (-)
γ_0	free space wave number (m^{-1})
κ	permeability (m^2)
λ	wavelength (m)
ρ	density (kg/m^3)
σ	electrical conductivity (S/m)
ϖ	angular frequency (rad/s)
ω	blood perfusion rate (1/s)
μ	dynamic viscosity (N.s/m^2)
μ_r	relative permeability (-)
Subscripts	
b	blood
ext	external
eff	effective
ref	reference
met	metabolic
n	normal
r	radial coordinate
s	solid
z	axial coordinate

CRediT authorship contribution statement

Teerapot Wessapan: Writing – review & editing, Writing – original draft, Project administration, Methodology, Investigation, Funding acquisition, Conceptualization. **Pornthip Keangin:** Writing – original draft, Visualization, Validation, Investigation, Formal analysis, Data curation. **Phadungsak Rattanadecho:** Supervision, Software, Project administration, Funding acquisition. **Nisakorn Somsuk:** Writing – review & editing, Resources.

Declaration of competing interest

Please declare for each author any conflicts of interest relevant to what you write.

This includes employment, consultancies, stock ownership, honoraria, paid expert testimony, patent applications and travel grants. If there are no conflicts of interest, please state that there are The authors declare that they have no known competing financial interests or personal relationships that could have appeared to influence the work reported in this paper.

Acknowledgments

This research was supported by the National Science, Research, and Innovation Fund, Thailand Science Research and Innovation (TSRI), through Rajamangala University of Technology Thanyaburi (FRB67E0707) (grant no FRB670027/0168) and the National Research Council of Thailand (grant no N42A650197).

Data availability

The authors do not have permission to share data.

References

[1] J. Wang, L. Wan, G. Huang, C. Chen, Y. Wu, Comparison of high-intensity focused ultrasound and microwave ablation for the treatment of small liver metastatic tumors, J. Int. Med. Res. 51 (4) (2023) 03000605231165551.

[2] S. Curto, M. Taj-Eldin, D. Fairchild, P. Prakash, Microwave ablation at 915 MHz vs 2.45 GHz: a theoretical and experimental investigation, Med. Phys. 42 (2015) 6152–6161.

[3] A.-R.A. Khaled, K. Vafai, The role of porous media in modeling flow and heat transfer in biological tissues, Int. J. Heat Mass Transf. 46 (2003) 4989–5003.

[4] H.H. Pennes, Analysis of tissue and arterial blood temperatures in the resting human forearm, J. Appl. Physiol. 1 (1948) 93–122.

[5] S. Mortazavi, M. Mokhtari-Dizaji, Numerical study of high-intensity focused ultrasound (HIFU) in fat reduction, Skin Res. Technol. 29 (1) (2023) e13280.

[6] H. Dong, G. Liu, G. Peng, Simulation study of the effects of HIFU irradiation patterns on thermal lesion to biological tissue, Sci. Iran. (2024), https://doi.org/10.24200/sci.2024.62707.7987.

[7] M. Selmi, A.A. Bin Dukhyil, H. Belmabrouk, Numerical analysis of human cancer therapy using microwave ablation, Appl. Sci. 10 (1) (2019) 211.

[8] C. Chen, M.A. Yu, L. Qiu, H.Y. Chen, Z.L. Zhao, J. Wu, L.L. Peng, Z.L. Wang, R. X. Xiao, Theoretical evaluation of microwave ablation applied on muscle, fat and bone: a numerical study, Appl. Sci 11 (17) (2021) 8271.

[9] C. Tucci, M. Trujillo, E. Berjano, M. Iasiello, A. Andreozzi, G.P. Vanoli, Pennes' bioheat equation vs. porous media approach in computer modeling of radiofrequency tumor ablation, Sci. Rep 11 (1) (2021) 5272.

[10] M. Mohammadpour, B. Firoozabadi, High intensity focused ultrasound (HIFU) ablation of porous liver: numerical analysis of heat transfer and hemodynamics, Appl. Therm. Eng. 170 (2020) 115014.

[11] M. Sadeghi-Goughari, S. Jeon, H.J. Kwon, Analytical and numerical model of high intensity focused ultrasound enhanced with nanoparticles, IEEE Trans. Biomed. Eng. 67 (11) (2020) 3083–3093.

[12] T. Wessapan, P. Rattanadecho, Acoustic streaming effect on flow and heat transfer in porous tissue during exposure to focused ultrasound, Case Stud, Therm. Eng. 21 (2020) 100670.

[13] P. Keangin, P. Rattanadecho, A numerical investigation of microwave ablation on porous liver tissue, Adv. Mech. Eng. 10 (6) (2018) 1–13.

[14] W. Preechaphonkul, V. Mongkol, A. Sakonkanapong, P. Rattanadecho, Numerical analysis of heat transfer and tissue deformation in liver cancer during microwave ablation: a comparison of bioheat and porous media models, (2024). Available at https://doi.org/10.2139/ssrn.4978787.

[15] S. Hossain, S.M.C. Hossain, M. Ferdows, M.Z.I. Bangalee, M.S. Alam, Computer simulation based analysis of transient two-phase thermal evolutions during multiprobe cryosurgery of hepatic tissues embedded without or with blood vessels, Int. J. Thermofluids 21 (2024) 100587.
[16] G. Shankar, E.P. Siva, D. Tripathi, O.A. Beg, Thermal analysis in unsteady oscillatory Darcy blood flow through stenosed artery, Int. J. Thermofluids 24 (2024) 100864.
[17] M.A. Rahman, H.J. Apon, M. Rabbani, M.H. Maruf, A.S.M. Shihavuddin, Numerical simulation and analysis of the temporal concentration of timolol after topical administration in the human eye, Int. J. Thermofluids 16 (2022) 100251.
[18] S. Ahmad, F. Ali, I. Khan, S.U. Haq, Biomedical applications of gold nanoparticles in thermofluids flow through a porous medium, Int. J. Thermofluids 20 (2023) 100425.
[19] E.E. Bafe, M.D. Firdi, L.G. Enyadene, Magnetohydrodynamic thermo-bioconvective flow of 3D rotating Williamson nanofluid with Arrhenius activation energy in a Darcy–Forchheimer medium over an exponentially stretching surface, Int. J. Thermofluids 21 (2024) 100585.
[20] A. Khalid, I. Khan, A. Khan, S. Shafie, I. Tlili, Case study of MHD blood flow in a porous medium with CNTS and thermal analysis, Case Stud, Therm. Eng. 12 (2018) 374–380.
[21] T. Wessapan, P. Rattanadecho, Flow and heat transfer through a porous tumor during high-intensity focused ultrasound, Int. J. Heat Mass Transf. 216 (2023) 124501.
[22] R. Bhowmik, S. Repaka, C. Mishra, K. Mitra, Thermal assessment of ablation limit of subsurface tumor during focused ultrasound and laser heating, J. Therm. Sci. Eng. Appl. 8 (2016) 011012. –1.
[23] H.C. Brinkman, A calculation of the viscous force exerted by a flowing fluid on a dense swarm of particles, Appl. Sci. Res. 1 (1949) 27–34.
[24] J. Huang, R.G. Holt, R.O. Cleveland, R.A. Roy, Experimental validation of a tractable numerical model for focused ultrasound heating in flow-through tissue phantom, Acoust. Soc. Am. 116 (4) (2004) 2451–2458.
[25] D. Yang, M.C. Converse, D.M. Mahvi, J.G. Webster, Expanding the bioheat equation to include tissue internal water evaporation during heating, IEEE Trans. Biomed. Eng. 54 (8) (2007) 1382–1388.